Articles

Evolution of Local Structure around Manganese in Layered $LiMnO_2$ upon Chemical and Electrochemical Delithiation/Relithiation

Seong-Ju Hwang, Hyo-Suk Park, and Jin-Ho Choy*

National Nanohybrid Materials Laboratory, and School of Chemistry and Molecular Engineering, Seoul National University, Seoul 151-742, Korea

Guy Campet

Institut de Chimie de la Matière Condensée de Bordeaux (ICMCB) du CNRS, Château Brivazac, Avenue du Dr. A. Schweitzer, 33608 Pessac, France

Received August 23, 1999. Revised Manuscript Received January 25, 2000

Mn K-edge X-ray absorption spectroscopic (XAS) analyses have been performed to probe the evolution of electronic and crystal structures of layered $LiMnO_2$ upon chemical and electrochemical delithiation/relithiation. According to the X-ray absorption near-edge structure studies, it becomes clear that the trivalent manganese ion in $LiMnO_2$ is significantly oxidized by acid treatment and is not fully recovered by subsequent lithiation reaction with *n*-BuLi. The extended X-ray absorption fine structure results presented here demonstrate that the local structure around manganese in $LiMnO_2$ is changed from a layered α-$NaFeO_2$-type structure to a spinel-like one upon chemical delithiation reaction. It is also found from the XAS analyses for the cycled $LiMnO_2$ that the electrochemical charge−discharge process gives rise not only to the partial oxidation of manganese ion but also to the migration of Mn into the interlayer lithium site, resulting in the coexistence of the layered structure and the spinel one. Such results highlight the lattice instability of layered manganese oxide for the chemical and electrochemical extraction of lithium, which is responsible for the remarkable capacity fading and the formation of two plateaus at around the 3 and 4 V regions after the first electrochemical cycle. On the basis of the present experimental findings, we are now able to suggest that the electrochemical performance of layered $LiMnO_2$ can be improved by blocking the Mn migration path through cationic substitution.

Introduction

The spinel lithium manganate has attracted intense research interest as a prospective cathode material in lithium secondary batteries not only due to the low cost and low toxicity of manganese but also due to the facile synthesis of this phase.[1] Despite such advantages, the commercialization of $LiMn_2O_4$ spinel oxide has been frustrated by some serious defects such as inferior theoretical capacity and unacceptable capacity loss.[2] To overcome these shortcomings of manganese oxide, a new layered $LiMnO_2$ oxide has recently been developed as an alternative cathode material through the ion-exchange reaction between α-$NaMnO_2$ and LiBr (or LiCl).[3,4] Although this compound exhibits a large initial capacity of more than 270 mAh/g, it also suffers from severe capacity fading like the spinel $LiMn_2O_4$ phase.[3] In this regard, it is quite important to elucidate the effect of the lithium deintercalation−intercalation process on the crystal structure of layered $LiMnO_2$ in understanding the mechanism responsible for capacity fading and in improving the electrochemical performance of this compound. For this reason, neutron and X-ray diffraction (XRD) studies have been performed for the cycled derivatives of $LiMnO_2$,[5,6] revealing that the α-$NaFeO_2$-type layered structure of the pristine compound is insignificantly modified by the first charge process. This must be contrasted with electrochemical measurements where a remarkable decrease in capacity is observed just after the first charge process.[5] Such an inconsistency between both experiments could be attributed to the fact that the diffraction tools cannot

* To whom correspondence should be addressed. Telephone: +82-2-880-6658. Fax: +82-2-872-9864. E-mail: jhchoy@plaza.snu.ac.kr.

(1) Thackeray, M. M.; David, W. I. F.; Bruce, P. G.; Goodenough, J. B. *Mater. Res. Bull.* **1983**, *18*, 461.
(2) Thackeray, M. M. *Prog. Solid State Chem.* **1997**, *25*, 1.
(3) Armstrong, A. R.; Bruce, P. G. *Nature* **1996**, *381*, 499.
(4) Capitaine, F.; Gravereau, P.; Delmas, C. *Solid State Ionics* **1996**, *89*, 197.
(5) Bruce, P. G.; Armstrong, A. R.; Gitzendanner, R. L. *J. Mater. Chem.* **1999**, *9*, 193.
(6) Vitins, G.; West, K. *J. Electrochem. Soc.* **1997**, *144*, 2587.

10.1021/cm9905491 CCC: $19.00
Published on Web 07/17/2000

Table 1. Lattice Parameters, Crystal Symmetries, and Chemical Formulas of Layered $LiMnO_2$, Acid-Treated $LiMnO_2$, λ-MnO_2, *n*-BuLi-Treated $LiMnO_2$, and Spinel $LiMn_2O_4$

sample	*a* (Å)	*b* (Å)	*c* (Å)	*c*/*a*	β (deg)	crystal symmetry	chemical formula
$LiMnO_2$	5.443	2.810	5.392	0.99	116.012	monoclinic	$Li_{1.02}MnO_2$
acid-treated $LiMnO_2$	2.859		13.378	4.68		rhombohedral	$Li_{0.00}H_{0.34}MnO_2$
λ-MnO_2	8.040					cubic	$Li_{0.03}H_{0.06}MnO_2$
n-BuLi-treated $LiMnO_2$[a]	8.234					cubic	$Li_{0.36}H_{0.25}MnO_2$
$LiMn_2O_4$	8.237					cubic	$Li_{1.07}Mn_2O_4$

[a] The relithiated product $Li_{0.36}H_{0.25}MnO_2$ was prepared by reacting the delithiated $H_{0.34}MnO_2$ with 1.6 M *n*-BuLi solution.

provide information on the local structural change induced by electrochemical cycling but reflects the average crystal structure of this electrode material. In this respect, recently transmission electron microscopic (TEM) studies have been performed for the layered $LiMnO_2$ and its electrochemically cycled derivatives, which indicated the modification of layered structure to spinel one just after the first charge process.[7,8]

In this work, we have applied X-ray absorption spectroscopy (XAS) to investigate the variation in the chemical bonding environment around manganese upon electrochemical cycling, since this tool allows us to quantitatively determine the local structure and electronic configuration of absorbing atoms even for the poorly crystallized solids. Actually XAS has been widely used to investigate the intercalation mechanism of diverse cathode materials such as $LiMn_2O_4$, $LiNi_{1-x}Ti_xO_2$, $LiNi_{1-x}Co_xO_2$, etc.[9−16] In addition to the electrochemical cycling, we have also studied the chemical lithium deintercalation/reintercalation reactions via acid and *n*-BuLi treatments. Such reactions have been extensively studied to clarify the structural modification of $LiMn_2O_4$ spinel upon Li deintercalation/intercalation as well as to probe its applicability as a lithium-selective ion sieve.[17−19] However, for the layered $LiMnO_2$ oxide under investigation, the effect of acid and *n*-BuLi treatments on its crystal and electronic structures has not been reported yet, even though the completely/partially deintercalated Li_xMnO_2 ($0 \le x \le 1$) phases were previously prepared by electrochemical methods.[5] In this regard, we have also carried out XRD and XAS studies on the acid- and *n*-BuLi-treated layered $LiMnO_2$ compounds to investigate the evolution of the chemical bonding character upon chemical extraction and reinsertion of lithium.

Experimental Section

Sample Preparation. A polycrystalline sample of $LiMnO_2$ was prepared by ion exchange reaction of α-$NaMnO_2$ with LiBr, as reported previously.[3] The single phase α-$NaMnO_2$ was obtained by heating the mixture of Na_2CO_3 and Mn_2O_3 (mole ratio = 1.1:1.0) at 725 °C for 40 h with intermittent grindings. And the ion exchange reaction was performed by heating α-$NaMnO_2$ in an *n*-hexanol solution of lithium bromide (10 mol excess) at 148 °C for 48 h. The brownish precipitate was filtered, washed with *n*-hexanol and methanol, and dried in a vacuum. In contrast to the very hygroscopic nature of the precursor α-$NaMnO_2$, the resulting $LiMnO_2$ was found to be rather stable in an ambient atmosphere. The chemical delithiation reaction was carried out by stirring $LiMnO_2$ with 2.5 M H_2SO_4 solution for 48 h,[20] and then the lithium was reinserted by reacting the delithiated sample with 1.6 M *n*-BuLi in hexane for 48 h. Prior to the physicochemical characterization, both the delithiated and relithiated samples were washed thoroughly with distilled water and methanol, and dried at 80 °C in air.

Sample Characterization. The effects of chemical delithiation and relithiation on the crystal structure of layered $LiMnO_2$ were studied by XRD measurement using Ni-filtered Cu Kα radiation with a graphite diffracted beam monochromator. The chemical compositions of these samples were determined by performing atomic absorption (AA) spectrometry. For the delithiated and relithiated products, thermogravimetric analysis (TGA) was also carried out to check out the possibility of proton intercalation during acid treatment. From the weight loss for the temperature region 150−300 °C corresponding to the dehydroxylation reaction,[19] the amount of inserted proton could be calculated. As listed in Table 1, the present AA and TGA results revealed that all the lithium in $LiMnO_2$ is extracted by acid treatment, but a considerable number of protons are incorporated into the layered structure, which is contrasted with λ-MnO_2.[19] Such prominent incorporation of protons into the layered structure could be understood as follows: in contrast to the three-dimensional spinel network, the layered structure of $LiMnO_2$ becomes unstable upon extraction of interlayer lithium ions through the enhancement of electrostatic repulsion between adjacent oxide layers, which can be relieved by inserting the proton into the interlayer space. To understand the lithium extraction mechanism during acid treatment, we have also measured the concentration of Mn ion in the residual acidic solution used for delithiation reaction, which revealed that 0.43 Mn per unit formula is dissolved during acid treatment. In light of this, the following delithiation reaction can be established: $LiMn^{+III}O_2 + 0.9H_2SO_4 \rightarrow 0.6H_{0.34}Mn^{+III}_{0.34}Mn^{+IV}_{0.66}O_2 + 0.4MnSO_4 + 0.5Li_2SO_4 + 0.8H_2O$.

On the other hand, the electrochemical measurements were performed with the cell of Li/1 M $LiPF_6$ in EC:DEC (50:50 v/v)/$LiMnO_2$, which was assembled in a drybox. The composite cathode was prepared by mixing thoroughly the active $LiMnO_2$

(7) Shao-Horn, Y.; Hackney, S. A.; Armstrong, A. R.; Bruce, P. G.; Gitzendanner, R.; Johnson, C. S.; Thackeray, M. M. *J. Electrochem. Soc.* **1999**, *146*, 2404.
(8) Wang, H.; Jang, Y. I.; Chiang, Y.-M. *Electrochem. Solid State Lett.* **1999**, *2*, 490.
(9) Choy, J. H.; Kim, D. H.; Kwon, C. W.; Hwang, S. J.; Kim, Y. I. *J. Power Sources* **1999**, *77*, 1.
(10) Treuil, N.; Labrugère, C.; Menetrier, M.; Portier, J.; Campet, G.; Deshayes, A.; Frison, J. C.; Hwang, S. J.; Song, S. W.; Choy, J. H. *J. Phys. Chem. B* **1999**, *103*, 2100.
(11) Chang, S. H.; Kang, S. G.; Song, S. W.; Yoon, J. B.; Choy, J. H. *Solid State Ionics* **1996**, *86*−*88*, 171.
(12) Ammundsen, B.; Jones, D. J.; Rozière, J.; Burns, G. R. *Chem. Mater.* **1996**, *8*, 2799.
(13) Ammundsen, B.; Jones, D. J.; Rozière, J. *J. Solid State Chem.* **1998**, *141*, 294.
(14) Shiraishi, Y.; Nakai, I.; Tsubata, T.; Himeda, T.; Nishikawa, F. *J. Solid State Chem.* **1997**, *133*, 587.
(15) Yamaguchi, H.; Yamada, A.; Uwe, H. *Phys. Rev. B* **1998**, *58*, 8.
(16) Nakai, I.; Nakagome, T. *Electrochem. Solid-State Lett.* **1998**, *1*, 259.
(17) Hunter, J. C. *J. Solid State Chem.* **1981**, *39*, 142.
(18) Larcher, D.; Courjal, P.; Urbina, R. H.; Gerand, B.; Blyr, A.; Pasquier, A.; Tarascon, J. M. *J. Electrochem. Soc.* **1998**, *145*, 3392.7.
(19) Feng, Q.; Miyai, Y.; Kanoh, H.; Ooi, K. *Langmuir* **1992**, *8*, 1861.

(20) We have also tried to extract the lithium under milder conditions (0.1 M HNO_3 solution), which results in the formation of mixed phases consisting of completely and partially delithiated domains.

cathode material (85%) with 10% of acetylene black and 5% of PTFE (poly(tetrafluoroethylene)). All the experiments were performed in a galvanostatic mode at a constant current density of 0.5 mA/cm^2 with an Arbin BT 2043 multichannel galvanostat/potentiostat with a voltage in the range of 2.2−4.3 V. A high initial capacity of ∼220 mAh/g was obtained for the first charge process, whereas it was significantly decreased to ∼110 mAh/g for the subsequent discharge process, as reported previously.[5] From the observed charge capacities, the chemical formula of the first cycled sample could be estimated to be $Li_{0.62}MnO_2$, with the supposition that the charge capacity on the charge−discharge process originates wholly from the lithium deintercalation−intercalation reaction.

X-ray Absorption Measurement. To probe the effects of chemical and electrochemical delithiation/relithiation reactions on crystal and electronic structures of layered lithium manganate, XAS experiments were performed for the pristine $LiMnO_2$ compound and its acid-treated, *n*-BuLi-treated, and electrochemically cycled derivatives using an extended X-ray absorption fine structure (EXAFS) facility installed at the beam line 7C at the Photon Factory in Tsukuba.[21] The sample after the first electrochemical cycling was mounted on the sample holder with Kapton window tape in an Ar-filled drybox, to protect it from humidity. The XAS measurements were carried out at room temperature in a transmission mode using gas-ionization detectors. All the present spectra were calibrated by measuring the spectrum of a Mn metal foil and by fixing the first absorption peak to 6539 eV. The data analysis for the experimental spectra was performed by the standard procedure reported previously.[9,10] All the present X-ray absorption near-edge structure (XANES) spectra were normalized by fitting the smooth EXAFS high-energy region with a linear function after subtracting the background extrapolated from the preedge region. The EXAFS oscillations were separated from the absorption background using a cubic spline background removal technique. The resulting $\chi(k)$ oscillations were weighted with k^3 to compensate for the diminishing amplitude of the EXAFS in the high-k region. For analyzing the EXAFS data, a nonlinear least-squares curve fitting was carried out on the Fourier-filtered coordination shells by minimizing the value of F ($F = [\sum k^6 (\chi_{cal} - \chi_{exp})^2]^{1/2}/n$, where the summation was performed over the data points (n) in the analyzed k range) with the use of well-known single scattering EXAFS theory.[22]

Results and Discussion

Powder XRD Analysis. The powder XRD patterns for the pristine $LiMnO_2$, acid-treated $LiMnO_2$, and *n*-BuLi-treated $LiMnO_2$ are represented in Figure 1, together with those for the spinel $LiMn_2O_4$ and λ-MnO_2,[23] and the lattice parameters obtained from the least-squares fitting analyses are summarized in Table 1. The XRD feature for the pristine $LiMnO_2$ is found to be the same as that for the layered α-$NaFeO_2$-type structure with a monoclinic distortion, while all the XRD peaks for $LiMn_2O_4$ and λ-MnO_2 can be well indexed on the basis of cubic spinel structure. Compared to the pristine $LiMnO_2$ compound, the acid-treated $LiMnO_2$ sample shows a simpler pattern which corresponds to the layered structure with a rhombohedral symmetry. Upon acid treatment, the (001) reflection of $LiMnO_2$ relating to the interlayer distance between MnO_2 layers is shifted to the (003) reflection of the acid-treated $LiMnO_2$ at a higher angle, indicating the lattice contraction caused by lithium deintercalation.[24] In fact, the present XRD pattern for the acid-treated sample is revealed to be nearly the same as the previously reported pattern for an electrochemically charged sample,[5] confirming that the acid treatment can also lead to an extraction of lithium. On the other hand, the lithiation reaction with *n*-BuLi leads to a low-angle shift of the (003) peak for the delithiated $LiMnO_2$, suggestive of reinsertion of lithium into the manganate lattice with a lattice expansion. However, its position is still higher compared to the (001) peak of the pristine $LiMnO_2$, which implies not all the deintercalated lithium is reinserted by the reaction with *n*-BuLi. This is in good agreement with the present AA results (Table 1). The overall XRD pattern of the relithiated sample is observed to be rather similar to that of the spinel $LiMn_2O_4$, suggesting that it would possess a spinel-like crystal structure. On the other hand, this pattern can be also indexed on the basis of a rhombohedral layered structure with a c/a ratio of 4.92 (a = 2.902 Å, c = 14.275 Å). Considering the fact that a rhombohedral cell with a c/a ratio of 4.9 is equivalent crystallographically to a cubic cell,[25] this would support the transition from the layered structure to the spinel one upon lithiation reaction. However, here we are unable to obviously assign the present XRD pattern as the layered or spinel structures, since its low signal-to-noise (S/N) ratio prevents from the profile refinements. As shown in Figure 1, the acid- and

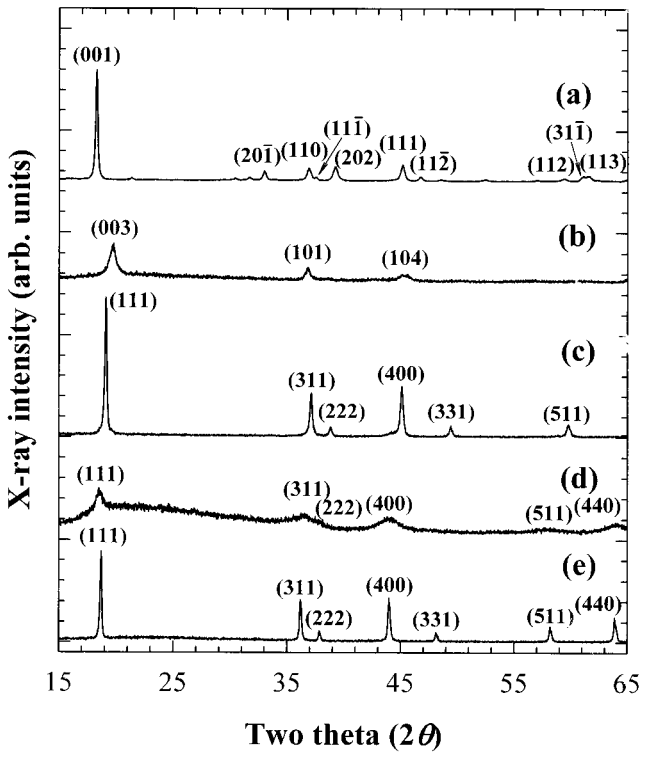

Figure 1. Powder XRD patterns for (a) the layered $LiMnO_2$, (b) the acid-treated $LiMnO_2$, (c) λ-MnO_2, (d) the *n*-BuLi-treated $LiMnO_2$, and (e) $LiMn_2O_4$.

(21) Oyanagi, H.; Matsushida, T.; Ito, M.; Kuroda, H. *KEK Report* **1984**, *83*, 30.

(22) Teo, B. K. *EXAFS: Basic Principles and Data Analysis*; Springer-Verlag: Berlin, 1986.

(23) As references for XRD and XAS analyses, the spinel $LiMn_2O_4$ compound was prepared by solid-state reaction at 800 °C and λ-MnO_2 was synthesized by reacting $LiMn_2O_4$ with 2.5 M H_2SO_4 solution for 48 h.

(24) The diffraction of an X-ray beam originating from the basal plane gives rise to the most intense peak in all the present XRD patterns, namely, (001) reflection for $LiMnO_2$, (003) reflection for acid-treated $LiMnO_2$, and (111) reflection for *n*-BuLi-treated $LiMnO_2$ and $LiMn_2O_4$.

(25) Cullity, B. D. *Elements of X-ray Diffraction*, Addison-Wesley: 1978.

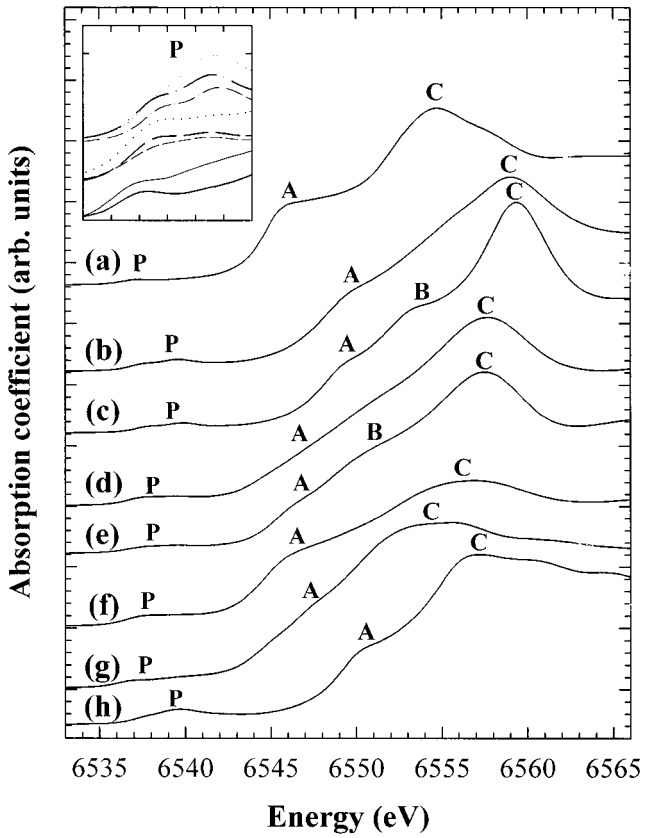

Figure 2. Mn K-edge XANES spectra for (a) the layered $LiMnO_2$ (thick solid lines), (b) the acid-treated $LiMnO_2$ (thick dot−dashed lines), (c) λ-MnO_2 (thin dot−dashed lines), (d) the *n*-BuLi-treated $LiMnO_2$ (thick dashed lines), (e) $LiMn_2O_4$ (thin dashed lines), (f) electrochemically cycled $LiMnO_2$ (thick dotted lines), in comparison with those for the references (g) Mn_2O_3 (thin solid lines) and (h) MnO_2 (thin dotted lines). The information in parentheses is for the curves in the inset. The inset provides enlarged views of all the present spectra with an energy range of 6535−6541 eV. For the clear presentation of spectral features in the preedge region, the spectra of the acid-treated $LiMnO_2$, λ-MnO_2, and MnO_2 in inset are shifted by 0.12 along the *y* axis while those of the *n*-BuLi-treated $LiMnO_2$, electrochemically cycled $LiMnO_2$, and $LiMn_2O_4$ are displaced by 0.06.

n-BuLi-treated derivatives of $LiMnO_2$ show much weaker and broader XRD peaks than the spinel $LiMn_2O_4$ and λ-MnO_2 phases, which underlines that the delithiation and lithiation processes at room temperature frustrate the long-range structural order.

Mn K-Edge XANES Analysis. The effects of chemical and electrochemical delithiation/relithiation upon electronic and geometric structures of manganese in layered $LiMnO_2$ have been investigated by performing XANES analyses. The Mn K-edge XANES spectra of the layered $LiMnO_2$, acid-treated $LiMnO_2$, λ-MnO_2, *n*-BuLi-treated $LiMnO_2$, $LiMn_2O_4$, and electrochemically cycled $LiMnO_2$ are plotted in Figure 2, in comparison with those for the reference cases of Mn_2O_3 and MnO_2. While the pristine $LiMnO_2$ exhibits nearly the same edge energy as $Mn^{+III}{}_2O_3$, the position of the edge jump for the acid-treated $LiMnO_2$ is quite a bit higher than that for $Mn^{+III}{}_2O_3$ but slightly lower than those for λ-MnO_2 and $Mn^{+IV}O_2$, which indicates that the trivalent manganese ion in $LiMnO_2$ is partially oxidized after acid treatment. Such a mixed oxidation state of manganese (Mn^{+III}/Mn^{+IV}) in the latter compound is ascribed mainly to the accompanying incorporation of protons rather than to the incomplete removal of interlayer lithium, as evidenced from the AA and TGA results. On the other hand, there is good consistency in the edge position between the *n*-BuLi-treated $LiMnO_2$ and the spinel $LiMn_2O_4$, revealing that the Mn valencies for both compounds are 3.5 in average. Upon electrochemical charge−discharge processes, the edge position is shifted toward the higher energy side, which indicates the increase of Mn oxidation state due to the irreversibility of the lithium deintercalation/intercalation.[3,6] All the spectra presented here show a small preedge peak (denoted P), which is assigned to the transition from the core 1s level to unoccupied 3d states.[10] Even though it is not allowed by the electronic dipolar selection rule, $\Delta l = \pm 1$, the preedge peak P could be discerned either due to a quadrupole-allowed transition and/or due to a mixing of 4p and 3d states.[26] In this context, the weak intensity of this peak suggests that all the manganese ions in the samples under investigation are stabilized in octahedral site with an inversion center. The position and shape of this preedge peak are well-known to be closely related to the oxidation state of the absorbing ion and the local arrangement of backscattering ions, respectively.[10] For this reason, the spectral features in the preedge region have been carefully investigated to obtain detailed information on the electronic and geometric structures of the manganese−oxygen layer, as shown in the inset of Figure 2. It is certain that the layered $LiMnO_2$ has a peak position similar to that of Mn_2O_3, whereas the peak energy of the acid-treated compound is quite a bit higher than that of Mn_2O_3 but lower than those of λ-MnO_2 and MnO_2. And upon relithiation with *n*-BuLi, this feature is displaced again toward the lower energy side, leading to the similar peak energy to the spinel $LiMn_2O_4$. In the case of electrochemically cycled sample, the energy of this peak is slightly higher compared to the pristine $LiMnO_2$, confirming the irreversible deintercalation/intercalation of lithium.[3,6] For all the present compounds, the relative energies of preedge peaks are wholly consistent with the order of the main-edge positions. In addition to the peak shift, its spectral features are also significantly altered after chemical and electrochemical delithiation/relithiation reactions, demonstrating a modification of the local cation ordering around manganese. A slight enhancement of preedge peak is detected for these chemically/electrochemically modified $LiMnO_2$ samples with respect to the spinel phases, i.e., λ-MnO_2 and $LiMn_2O_4$. This implies that the chemical and electrochemical delithiation/relithiation reactions at room temperature considerably increase the local structural disorder around manganese ions, resulting in a frustration of inversion symmetry. In the main-edge region, there are two or three fine features (denoted A, B, and C), those which are assigned as the dipole-allowed transitions from the core 1s level to unoccupied 4p states. While the characteristic peak A has considerable intensity for the layered $LiMnO_2$ compound, the intensity appears to be much weaker for the other samples presented here. Generally the fine structures in the XANES region sensitively reflect the local structure around an absorbing atom since they originate from the multiple scat-

(26) Grunes, L. A. *Phys. Rev. B* **1983**, *27*, 2111.

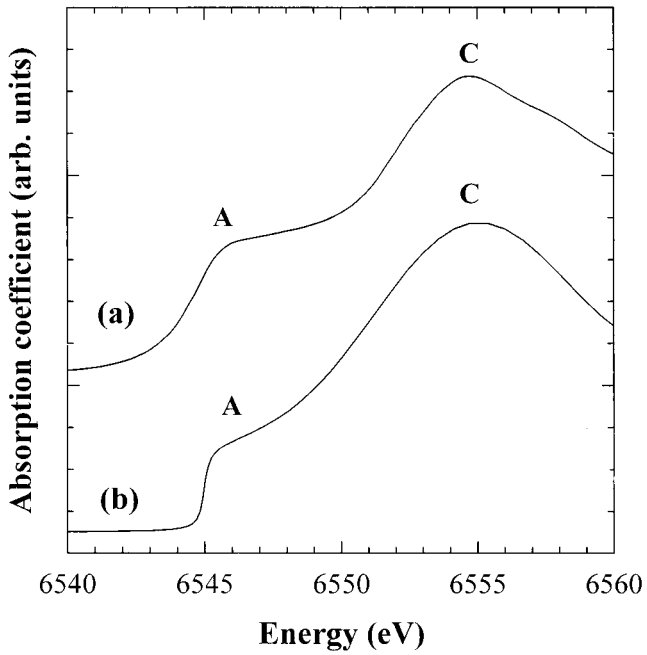

Figure 3. Comparison of (a) experimental and (b) simulated Mn K-edge XANES spectra of the layered $LiMnO_2$. The simulated spectrum was shifted by 4.8 eV in order to compensate the energy difference from the experimental spectrum which originates from ignoring the Mn oxidation state in the simulation procedure.

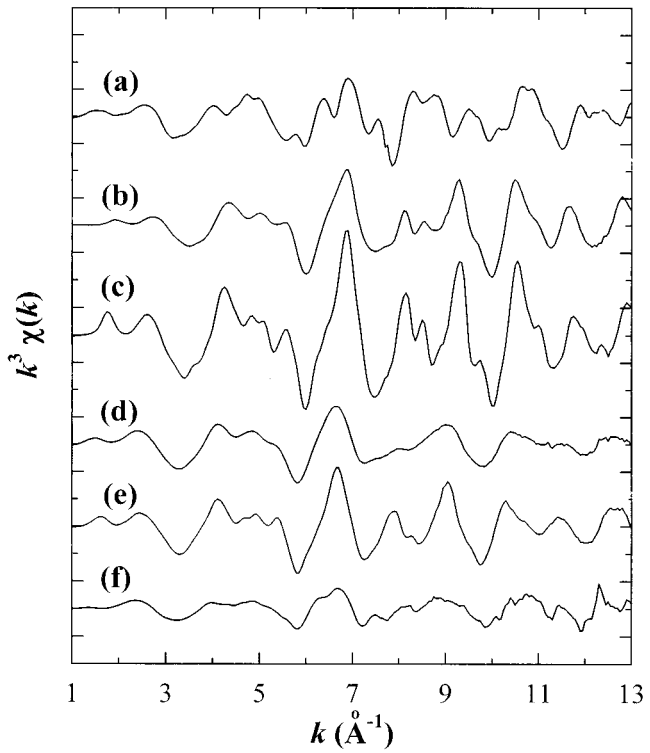

Figure 4. Experimental k^3-weighted Mn K-edge EXAFS spectra for (a) the layered $LiMnO_2$, (b) the acid-treated $LiMnO_2$, (c) λ-MnO_2, (d) the *n*-BuLi-treated $LiMnO_2$, (e) $LiMn_2O_4$, and (f) electrochemically cycled $LiMnO_2$.

tering of ejected photoelectrons by backscatterers and/or from the electronic transition to the localized states whose energies are also closely related to the atomic arrangement of neighboring atoms.[27] In light of this, an attempt has been made to reproduce theoretically the spectrum of layered $LiMnO_2$ by performing an ab-initio calculation with FEFF 6.0 code (Figure 3).[28] The theoretical XANES spectrum simulating over 41 coordination shells with 278 paths up to 6.7 Å coincides well with the experimental one.[29] Such an intense peak A has also been reported for the tetragonal $Li_2Mn_2O_4$ spinel phase.[30] In this respect, the observation of the strong peak A can be regarded as an indication of a Jahn−Teller active Mn^{+III} ion stabilized in a tetragonally distorted octahedron in a monoclinic layered or tetragonal spinel lattice. As illustrated in Figure 2, peak A is notably depressed upon acid treatment and is not recovered by the following lithiation process, which indicates that the local structure of manganese in a layered $LiMnO_2$ compound experiences the irreversible modification during chemical delithiation/relithiation reactions. In the case of the cycled derivative, a distinct feature A is much more prominent than that of the chemically delithiated or relithiated $LiMnO_2$ compound. Such a finding allows us to conjecture that a considerable amount of the layered (or tetragonal spinel) structure exists even after electrochemical cycling. Actually, the recent TEM analysis revealed that the electrochemical cycling results in the mixed phases of monoclinic layered structure and cubic (tetragonal) spinel one.[7] In this regard, we have tried to reproduce the experimental XANES spectrum of the cycled $LiMnO_2$ by mixing the data of the pristine $LiMnO_2$ and the spinel $LiMn_2O_4$. The calculated spectrum with a mixing ratio of 6:4 for layer:spinel (not shown) is revealed to be quite similar to the experimental one of the cycled derivative, even though the peaks in the former are rather sharper than those in the latter. Such a difference in peak sharpness can be well understood by considering that the mixed phase consisting of spinel and layered domains causes a considerable disorder in the local cation ordering around manganese, leading to a broadening of the fine structures in the XANES region.

Mn K-Edge EXAFS Analysis. The variations in the crystal structure of the layered $LiMnO_2$ compound upon chemical and electrochemical delithiation/relithiation processes have been examined quantitatively using Mn K-edge EXAFS spectroscopy. The k^3-weighted Mn K-edge EXAFS spectra for the layered $LiMnO_2$, acid-treated $LiMnO_2$, λ-MnO_2, *n*-BuLi-treated $LiMnO_2$, $LiMn_2O_4$, and electrochemically cycled $LiMnO_2$ are represented in Figure 4, and the corresponding Fourier transforms (FTs) are in Figure 5. As can be seen from Figure 4, the overall spectral feature of EXAFS oscillation of the delithiated $LiMnO_2$ compound is quite similar to that of λ-MnO_2, whereas the relithiated $LiMnO_2$ compound exhibits almost the same oscillation as the spinel $LiMn_2O_4$. Since the experimental EXAFS signal contains all the contributions from the entire

(27) Choy, J.-H.; Kim, D.-K.; Hwang, S.-H.; Demazeau, G. *Phys. Rev.* B **1994**, *50*, 16631.

(28) Rehr, J.-J.; Mustre de Leon, J.; Zabinsky, S.-I.; Albers, R.-C. *J. Am. Chem. Soc.* **1991**, *113*, 5135−5140. Mustre de Leon, J.; Rehr, J.-J.; Zabinsky, S.-I.; Albers, R.-C. *Phys. Rev. B.* **1991**, *44*, 4146−4156. O'day, P.-A.; Rehr, J.-J.; Zabinsky, S.-I.; Brown, G.-E., Jr. *J. Am. Chem. Soc.* **1994**, *116*, 2938−2949.

(29) While the ab-initio simulation with second-order multiple scattering paths also provides a spectrum rather similar to the experimental one, the calculation with single scattering paths gives poorly reproduced data.

(30) Ammundsen, B.; Jones, D. J.; Rozière, J.; Villain, F. *J. Phys. Chem. B* **1998**, *102*, 7939.

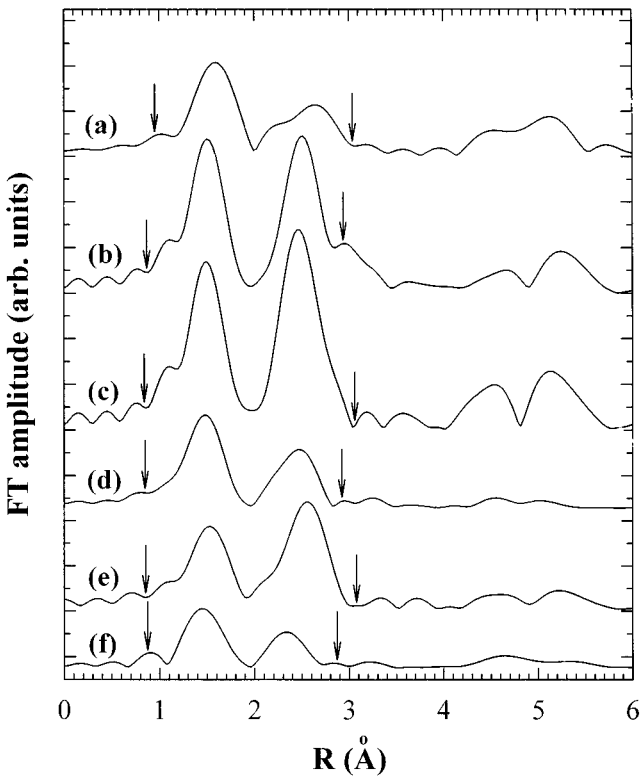

Figure 5. Fourier-transformed Mn K-edge EXAFS spectra for (a) the layered $LiMnO_2$, (b) the acid-treated $LiMnO_2$, (c) λ-MnO_2, (d) the *n*-BuLi-treated $LiMnO_2$, (e) $LiMn_2O_4$, and (f) electrochemically cycled $LiMnO_2$. The range over which the Fourier filtering has been made is shown by the arrows.

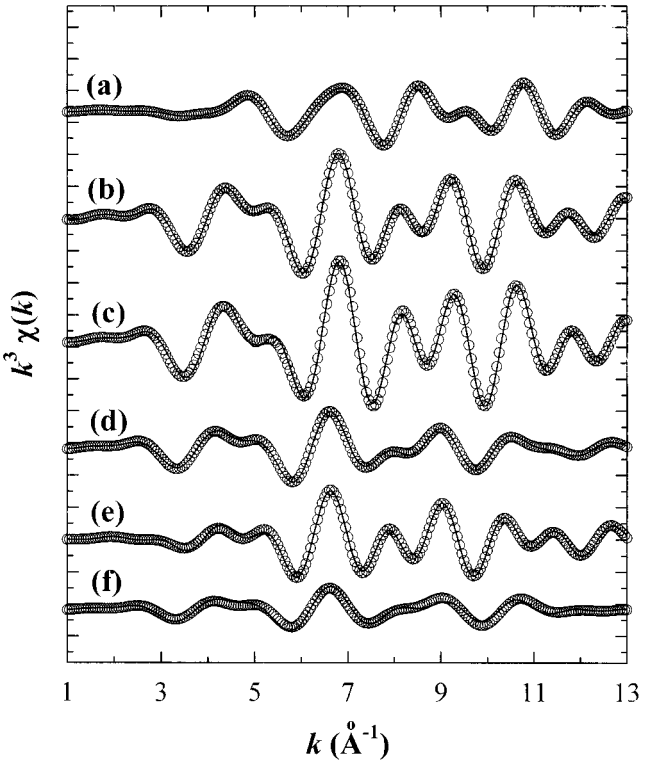

Figure 6. Comparison of the fitted spectra (solid lines) with the experimental data (empty circles) for (a) the layered $LiMnO_2$, (b) the acid-treated $LiMnO_2$, (c) λ-MnO_2, (d) the *n*-BuLi-treated $LiMnO_2$, (e) $LiMn_2O_4$, and (f) electrochemically cycled $LiMnO_2$.

scattering paths including single scatterings and multiple scatterings, the observed spectral similarities between the cubic spinel compounds and chemically treated $LiMnO_2$ derivatives suggest that both phases possess nearly the same local atomic arrangement. However, it should be noted here that if the delithiation reaction does not induce the migration of manganese ion, the delithiated $LiMnO_2$ derivative would be crystallized with the rhombohedral layered structure. It is therefore important to compare the present spectra of the $LiMnO_2$ derivatives with that of the rhombohedral layered structure. In this respect, we have theoretically simulated the EXAFS spectra of the rhombohedral $Li_{0.5}$-MnO_2 and MnO_2 phases, and compared them with the present experimental spectra of acid-treated and *n*-BuLi-treated $LiMnO_2$ compounds, and the theoretical/experimental spectra of spinel λ-MnO_2 and $LiMn_2O_4$ phases (not shown). From these comparisons, it becomes clear that the present spectra of the chemically treated $LiMnO_2$ derivatives are consistent with the theoretical/experimental spectra of cubic spinel phases, rather than the theoretical spectra of the rhombohedral layered $Li_{0.5}$-MnO_2 and MnO_2 oxides. This allows us to confirm the change of Mn local structure from the layered configuration to the spinel-like one after acid and *n*-BuLi treatments.[31] Such a structural variation caused by delithiation/relithiation reaction is further confirmed by our recent Raman study, in which the Raman spectra of acid- and *n*-BuLi-treated $LiMnO_2$ are found to be nearly the same as that of spinel oxide but they are different from that of layered lithium manganate with monoclinic or rhombohedral symmetry.[32] In the FT diagrams (Figure 5), the layered $LiMnO_2$ exhibits three intense FT peaks at ~1.6, ~2.2, and ~2.7 Å, those which are attributed to the (Mn−O), (Mn−Mn), and (Mn−Mn) shells, respectively, while two FT peaks corresponding to the (Mn−O) and (Mn−Mn) bonding pairs are discerned at ~1.5 and ~2.5 Å for both the spinel $LiMn_2O_4$ and λ-MnO_2. In the case of the acid- and *n*-BuLi-treated $LiMnO_2$, the overall spectral features are quite similar to the spinel λ-MnO_2 and $LiMn_2O_4$ rather than to the layered $LiMnO_2$. For both compounds, the magnitudes of the second FT peak intensities are found to be much smaller than those of the first FT ones, as reported for the spinel phase prepared at low temperature below 400 °C.[9,10] Such phenomena demonstrate that the delithiation/relithiation reactions give rise to a severe structural disorder in the distant coordination shells. These FT peaks were isolated by inverse Fourier transform to a *k* space. The resulting $k^3\chi(k)$ Fourier filtered EXAFS oscillations are represented in Figure 6, and curve fitting analyses were carried out for them to determine structural parameters such as the coordination number (*CN*), bond distance (*R*), and Debye−Waller factor (σ^2). As shown in Figure 6, the oscillation amplitudes of the chemically treated $LiMnO_2$ compounds are significantly smaller than those of spinel λ-MnO_2 and $LiMn_2O_4$ compounds. In general, there are two influences on the

(31) It is worthy to mention here that the EXAFS result for the delithiated product would be contrasted with the XRD one, which can be understood by the fact that the former probes the local atomic arrangement around manganese but the latter reflects the average crystal structure of this compound.

(32) Hwang, S. J.; Park, H. S.; Choy, J. H.; Campet, G.; Etourneau, J. To be published.

Table 2. Results of Nonlinear Least-Square Curve Fitting for the Mn K-Edge EXAFS Spectra of the Layered $LiMnO_2$, the Acid-Treated $LiMnO_2$, and the *n*-BuLi-Treated $LiMnO_2$, Together with the References of Spinel $LiMn_2O_4$ and λ-MnO_2

sample	bond	*CN* [a]	*R* (Å)	σ^2 ($10^{-3} \times$ Å^2)
$LiMnO_2$	(Mn−O_{eq})	4	1.91	1.69
	(Mn−O_{ax})	2	2.32	3.32
	(Mn−Mn)	2	2.80	3.00
	(Mn−Mn)	4	3.04	6.12
acid-treated	(Mn−O)	6	1.90	2.92
$LiMnO_2$	(Mn−Mn)	6	2.86	4.34
λ-MnO_2	(Mn−O)	6	1.90	3.19
	(Mn−Mn)	6	2.84	3.74
n-BuLi-treated	(Mn-O)	6	1.91	4.74
$LiMnO_2$	(Mn−Mn)	6	2.88	9.75
$LiMn_2O_4$	(Mn−O)	6	1.91	4.57
	(Mn−Mn)	6	2.91	5.00

[a] The coordination numbers (*CN*s) of all the present compounds have been calculated by using the amplitude reduction factor (S_0^2) of the reference $LiMn_2O_4$.

Table 3. Results of Nonlinear Least Square Curve Fitting for the Mn K-Edge EXAFS Spectrum of the Cycled $LiMnO_2$

sample	bond	CN	*R* (Å)	σ^2 ($10^{-3} \times$ Å^2)
cycled	$(Mn\text{-}O)_{spinel}$	3[c]	1.89	1.58
$LiMnO_2$[a]	$(Mn-Mn)_{spinel}$	3[c]	2.81	8.60
cycled	$(Mn-O_{eq})_{layer}$	4×0.6[d]	1.91	5.37
$LiMnO_2$[b]	$(Mn-O)_{spinel}$	6×0.4[d]	1.91	8.26
	$(Mn-O_{ax})_{layer}$	2×0.6[d]	2.32	18.43
	$(Mn-Mn)_{layer}$	2×0.6[d]	2.80	2.84
	$(Mn-Mn)_{spinel}$	6×0.4[d]	2.91	4.86
	$(Mn-Mn)_{layer}$	4×0.6[d]	3.04	5.95

[a] This EXAFS refinement has been performed on the basis of spinel structure. [b] This EXAFS refinement has been performed on the basis of the mixed structure consisting of layered and spinel phases. [c] The coordination numbers (*CN*s) of the cycled $LiMnO_2$ have been calculated by using the amplitude reduction factor (S_0^2) of the reference $LiMn_2O_4$. [d] The relative ratio of layered structure and spinel one in the cycled $LiMnO_2$ has been determined to be 6:4 by using the amplitude reduction factor (S_0^2) of the reference $LiMn_2O_4$.

amplitude in *k* space; one is the effect of coordination number whose increase enhances the signal in the entire *k* range, and the other is the effect of the Debye−Waller factor whose increase attenuates the amplitude at a high *k* region.[22] A closer inspection of Figure 6 reveals that the oscillation amplitude of the delithiated and relithiated derivatives decreases more prominently in a high *k* region than in a low *k* one, reflecting an increase of Debye−Waller factor. By taking into account the spectral similarity between chemically modified $LiMnO_2$ compounds and spinel phases, an attempt was made to fit each spectrum of delithiated and relithiated derivatives on the basis of the crystal structure of the spinel λ-MnO_2 and $LiMn_2O_4$, in such a way that we were able to obtain reasonable fitting results. The best fitting results are compared to the experimental spectra in Figure 6 and the fitted structural parameters are listed in Table 2.[33] The manganese ion in the layered $LiMnO_2$ is found to be stabilized in a tetragonally distorted octahedron with R(Mn−O_{eq}) = 1.91 Å and R(Mn−O_{ax}) = 2.32 Å, which is surely due to the Jahn−Teller distortion of trivalent manganese ions. Such a result is in good agreement with a previous neutron diffraction study.[3] The average (Mn−O) and (Mn−Mn) bond distances are estimated to be smaller for the acid-treated derivative than for the pristine $LiMnO_2$, confirming the increase of Mn oxidation state after acid treatment. And it is also observed that two different (Mn−O) bond distances are merged into a single value upon delithiation, which can be attributed to the disappearance of Jahn−Teller distortion induced by the oxidation of trivalent manganese ions. The shortened bond distances of the acid-treated $LiMnO_2$ are elongated again by reacting with *n*-BuLi, which is in accord with the low-energy shift of main edge in the XANES region. As listed in Table 2, the Debye−Waller factor of the second coordination shell becomes more significant for the delithiated/relithiated $LiMnO_2$ than for the pristine $LiMnO_2$ and the spinel λ-MnO_2/$LiMn_2O_4$, verifying a remarkable increase of structural disorder after acid and *n*-BuLi treatment. This is well correlated with the amorphization of crystal structure upon delithiation and relithiation processes, as evidenced from the XRD results presented above.

In the case of the electrochemically cycled $LiMnO_2$ derivative, the overall spectral features of the cycled $LiMnO_2$ are rather different from those of the pristine $LiMnO_2$ and the spinel $LiMn_2O_4$, pointing to that the local structure around manganese in $LiMnO_2$ is changed significantly after a charge−discharge cycle (Figures 4 and 5). The FT peaks were isolated by inverse Fourier transform to *k* space to perform the curve-fitting analyses (Figure 6). At first, an attempt was made to fit the experimental spectrum of the cycled derivative with the spinel structure. However, it gave physically meaningless fitting results, that is, $CN = 3$ for the (Mn−O) and (Mn−Mn) shells, indicating that the crystal structure of the cycled derivative is much more disordered than the cubic spinel phase. Alternatively, we have also tried to fit the experimental spectrum with monoclinic layered structure, only to failed. In light of the recent TEM study,[7] we have made an attempt to fit the spectrum of the cycled derivative based on the mixed structure consisting of monoclinic layered and cubic spinel phases. In this case, the best fitting results are obtained as shown in Figure 6 and the structural parameters obtained are listed in Table 3. In the course of the fitting analysis, the bond distances are fixed to the values determined from the EXAFS refinements for each $LiMnO_2$ and $LiMn_2O_4$ compound to obtain reasonable fitting results. The relative ratio of the monoclinic layer structure to the cubic spinel one is determined to be 6.3-(±0.4):3.7(±0.4), which highlights the fact that a considerable fraction of the layered-structure domain is altered to the spinel-type one following the electrochemical cycling process. This is supported by our recent Raman study where the electrochemical cycling is found to induce a partial formation of cubic spinel phase.[32] However, it is worth noting here that a partial fraction of tetragonal spinel $Li_2Mn_2O_4$ cannot be ruled out for the cycled sample, as supposed from the recent TEM analyses.[7] Considering the fact that the tetragonal spinel $Li_2Mn_2O_4$ would show nearly the same EXAFS oscillation as the layered $LiMnO_2$, the present value of

(33) Although both cubic spinel and rhombohedral layered structures possess the same chemical environments for the first and second coordination shells, the present structural parameters can be considered to correspond to the first and second shells of spinel phase, which is based on the spectral similarity between the EXAFS spectra of chemically treated $LiMnO_2$ samples and the cubic spinel ones as well as on the recent TEM and Raman studies.

6:4 would correspond to the relative ratio of layered and/or tetragonal spinel phases to cubic spinel one. On the other hand, judging from the chemical formula of this cycled sample, $Li_{0.62}MnO_2$, the above proportion of layer structure to spinel implies that the average lithium content (x) in the layered Li_xMnO_2 domain (or tetragonal spinel $Li_xMn_2O_4$ domain) is less than unity (or two).[34] This can be reasonably understood from the fact that the coexistence of spinel and layer domains would hinder the effective intercalation of lithium into the layer domain, which gives rise to an inhomogeneous distribution of lithium in this domain. On the other hand, the Debye−Waller factors of the cycled $LiMnO_2$ are found to be rather greater than the corresponding values obtained for each layer phase and spinel one, indicating a remarkable increase of structural disorder after cycling due to the coexistence of both phases. This is well correlated with the amorphization of crystal structure caused by the charge−discharge process.[5,6] Among the coordination shells of the cycled derivative, the axial (Mn−O) shell corresponding to the monoclinic layered structure (or tetragonal spinel one) shows a remarkably enhanced Debye−Waller factor, which is much greater than for the case of pure $LiMnO_2$ oxide. This is wholly consistent with our suggestion in which the severely lithiated domain would possess various levels of lithium content with several different (Mn−O_{ax}) bond distances. Summarizing the present experimental findings, it can be concluded that a significant local structural deformation is induced by the charge−discharge process, resulting in the coexistence of layered and spinel phases. Such a partial formation of spinel domains allows us to explain the significant decrease of charge capacity and the formation of two plateaus at around the 3 and 4 V regions in the first charge process.[5,6]

Modeling for Structural Modification upon Chemical and Electrochemical Delithiation. From the present XAS results for the chemically and electrochemically delithiated/relithiated $LiMnO_2$ compounds, it becomes clear that the extraction of lithium from the interlayer space leads to a partial formation of a spinel-like structure. This can be achieved by the migration of manganese ion into the lithium layer, as proposed from the previous electrochemical measurements and TEM study (Figure 7a).[5−8] Since such a structural change is surely responsible for the unfavorable capacity fading for the extended electrochemical cycling, it is expected that the cyclability of $LiMnO_2$ can be improved by preventing the migration of manganese ion. For this purpose, the mechanism for Mn migration during the electrochemical charge process needs to be elucidated. As illustrated in Figure 7b, the structural change from a layered structure to a spinel one can be accomplished by migrating one-fourth of the manganese ion in the MnO_2 block into the octahedral lithium site in the interlayer space, as supposed previously.[5,7] Since there are eight tetrahedral (T_d) sites near the octahedral (O_h) one in the edge-shared array of octahedra, two possible pathways can be proposed for Mn conduction into the corner-shared adjacent octahedra, that is, (1) $O_h \rightarrow T_d \rightarrow O_h \rightarrow T_d \rightarrow O_h$ and (2) $O_h \rightarrow O_h \rightarrow O_h$. Considering the available space for Mn conduction in the intermediate state,[35] the manganese ion can move more easily from O_h to T_d and vice versa, with respect to the $T_d \rightarrow T_d$ migration (or $O_h \rightarrow O_h$ one). In this light, path 1 is expected to be more energetically favorable than path 2, since the former contains no unfavorable $O_h \rightarrow O_h$ migration (or $T_d \rightarrow T_d$ one) while the latter includes two $O_h \rightarrow O_h$ ones. From the above discussion, it is suggested that following the delithiation process, the manganese ion in the MnO_2 block of $LiMnO_2$ moves into the octahedral lithium site in the interlayer space preferentially along the line of $O_h \rightarrow T_d \rightarrow O_h \rightarrow T_d \rightarrow O_h$. In this respect, it is expected that the electrochemical performance of layered $LiMnO_2$ can be improved by blocking this Mn migration path through cationic substitution, as observed for the spinel $LiMn_2O_4$.[36−38] Actually we have found that a partial substitution of Mn with Cr is effective in enhancing the electrochemical performance of layered $LiMnO_2$ compound.[39] Concurrently, it was also reported that the Al- (or Co-) substituted $LiMnO_2$ compound shows improved cyclability.[40,41] We are presently studying the role of Cr

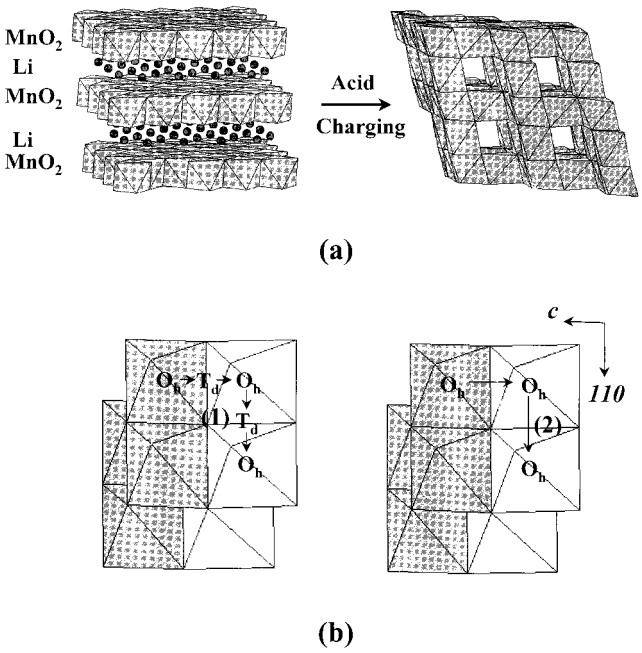

Figure 7. (a) Evolution of crystal structure of the layered $LiMnO_2$ upon acid treatment and electrochemical charging process and (b) the proposed migration paths of manganese ion from the O_h site in MnO_2 block into the interlayer lithium site. The shaded octahedra are occupied by manganese ions and the clear octahedra are occupied by lithium ions.

(34) If the layered and spinel domains possess the ideal compositions of $LiMnO_2$ and $LiMn_2O_4$, respectively, then the present relative ratio for both phases corresponds to the chemical formula of $Li_{0.8}MnO_2$.

(35) The manganese ion in an O_h site can move into the adjacent T_d site through the face of an MnO_6 octahedron, while for the $O_h \rightarrow O_h$ (or $T_d \rightarrow T_d$) migration, the Mn ion should pass through the center of an edge of an MnO_6 octahedron. The latter is expected to be much more unfavorable than the former, since the interatomic distance between two oxygens in the vertexes of an MnO_6 octahedron is too short for manganese ion to go through.

(36) Robertson, A. D.; Lu, S. H.; Averill, W. F.; Howard, W. F., Jr. *J. Electrochem. Soc.* **1997**, *144*, 3500.

(37) Arora, P.; Popov, B. N.; White, R. E. *J. Electrochem. Soc.* **1998**, *145*, 807.

(38) Sun, Y. K.; Jin, S. H. *J. Mater. Chem.* **1998**, *8*, 2399.

(39) Hwang, S. J.; Park, H. S.; Choy, J. H.; Campet, G. *J. Phys. Chem. B*, in press.

(40) Armstrong, A. R.; Gitzendanner, R.; Robertson, A. D.; Bruce, P. G. *Chem. Commun.* **1998**, 1833.

substitution in stabilizing the layer structure by using XRD, XAS, and Li NMR tools.

Conclusion

In the present study, an attempt has been made to investigate the effects of chemical and electrochemical delithiation/relithiation reactions on the electronic configuration and crystal structure of layered $LiMnO_2$ by performing systematic XAS analyses. According to the Mn K-edge XANES/EXAFS results presented here, it is certain that the chemical extraction and insertion of lithium give rise not only to the oxidation of trivalent manganese ion but also to a local structural change from a layered α-$NaFeO_2$-type structure to a spinel-like cation ordering. On the other hand, the XAS study for the cycled $LiMnO_2$ compound clarifies that the electrochemical cycling also induces the migration of manganese ions into the interlayer lithium site, resulting in the coexistence of layered and spinel structures with a ratio of 6:4. Such a structural modification allows us to explain the significant decrease of charge capacity and the formation of two plateaus at around the 3 and 4 V regions in the first charging process. On the basis of the present experimental findings, it was suggested that the cyclability of the layered $LiMnO_2$ can be improved by blocking the Mn migration path through cationic substitution, which has been confirmed by our recent study on Cr-substituted $LiMn_{1-x}Cr_xO_2$ compounds.

Acknowledgment. This work was supported in part by the Ministry of Science & Technology through 1999 National Research Laboratory (NRL) Project. Authors are grateful to Professor M. Nomura for helping us to obtain the XAS data in the Photon Factory. H.S.P. thanks the Ministry of Education for the Brain Korea 21 fellowship.

CM9905491

(41) Jang, Y. I.; Huang, B.; Chiang, Y.-M.; Sadoway, D. R. *Electrochem. Solid State Lett.* **1998**, *1*, 13.